

# Spin-polarized neutron reflectivity: A probe of vortices in thin-film superconductors

S.-W. Han

*Department of Physics and Astronomy, University of Missouri-Columbia, Columbia, Missouri 65211*

J. F. Ankner\* and H. Kaiser

*Missouri University Research Reactor, University of Missouri-Columbia, Columbia, Missouri 65211*

P. F. Miceli†

*Department of Physics and Astronomy, University of Missouri-Columbia, Columbia, Missouri 65211*

E. Paraoanu and L. H. Greene

*Department of Physics, University of Illinois at Urbana-Champaign, Urbana, Illinois 61801*

(Received 28 January 1999)

It is demonstrated that the specular reflectivity of spin-polarized neutrons can be used to study vortices in a thin-film superconductor. Experiments were performed on a 6000 Å thick *c*-axis film of  $\text{YBa}_2\text{Cu}_3\text{O}_{7-x}$  with the magnetic field applied parallel to the surface. A magnetic hysteresis loop was observed for the spin-polarized reflection and, from these data, the average density of vortices was extracted. A model is presented which relates the specular reflectivity to the one-dimensional spatial distribution of vortices in the direction perpendicular to the surface. Unlike other techniques, neutron reflectivity observes vortices in a geometry where they are parallel to the interface. [S0163-1829(99)07021-6]

## I. INTRODUCTION

The behavior of magnetic vortices, which form in a type II superconductor, is a subject of both fundamental and practical importance. The interaction between vortices as well as their interaction with pinning centers can lead to complex magnetic phase diagrams: vortices may order in a lattice or exhibit glassy or liquid behavior. These properties have been extensively studied in both conventional and high-temperature superconductors (HTC's).<sup>1-4</sup> Current-transport properties, which are central to technological applications of superconductors, strongly depend on the pinning of vortices.

For these reasons, there is considerable interest in having the capability to examine the spatial configuration of vortices. Several techniques have been used, including surface decoration with magnetic particles,<sup>5</sup> electron microscopy,<sup>6</sup> scanning tunneling microscopy,<sup>7</sup> Hall probe microscopy,<sup>8</sup> electron holography,<sup>9</sup> and small-angle neutron diffraction.<sup>4,10</sup> With the exception of the latter, these methods only image vortices at their point of exit through the surface. However, neutron diffraction requires both an ordered lattice of vortices as well as large-volume samples so that films cannot be studied.

Here, it is demonstrated that the specular reflection of spin-polarized neutrons can be used to study vortices in *thin-film* superconductors. The method makes the study of a unique geometry possible whereby vortices that run parallel to the surface can be investigated. Moreover, an ordered vortex lattice is not necessary for this technique. Although a uniform distribution of vortices is reported in the present experiments, it is shown that the technique is sensitive to a nonuniform vortex distribution in the direction perpendicular to the surface. With these capabilities it should be possible to investigate the interaction of vortices with interfaces.

Spin-polarized neutron reflectivity has been used extensively to study the structure and magnetism of thin magnetic layers.<sup>11</sup> The technique has also been applied to measure the London penetration depth  $\lambda_L$  in conventional<sup>12,13</sup> as well as HTC superconductors.<sup>14</sup> Figure 1 illustrates the essential

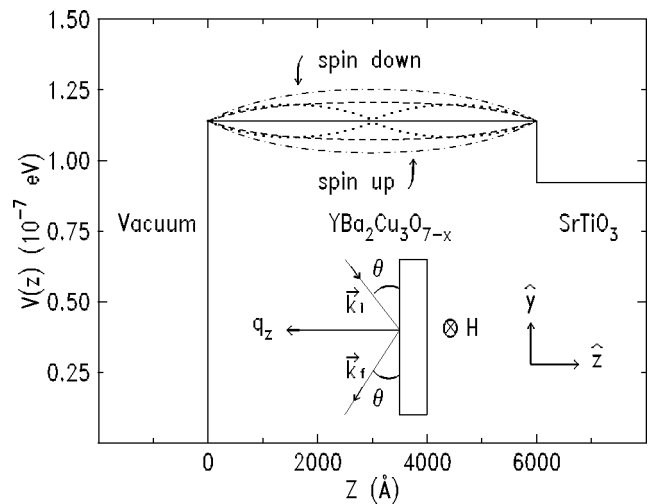


FIG. 1. Spin-up and spin-down neutrons encounter a different scattering potential due to the spatially varying magnetization in the superconductor. The scattering potential is calculated for: (Solid line) nuclear scattering only, (dot-dashed curve) London penetration without vortices, (dotted curve) vortices in the center of the sample, (dashed curve) uniform distribution of vortices. In each case, the lower branch is for spin-up neutrons and the upper branch is for spin-down neutrons. The inset shows the scattering geometry where the field is applied parallel to the surface, perpendicular to the scattering plane which is defined by the incident  $\vec{k}_i$  and outgoing  $\vec{k}_f$  wave vectors.

ideas for understanding neutron reflection from a superconductor. Because of the specular reflection geometry the momentum transfer  $q_z = (4\pi/\lambda)\sin\theta$  is perpendicular to the surface and the reflection process is determined by a 1D potential,  $V(z)$ , which contains contributions from both nuclear and magnetic scattering. When the magnetization and the neutron spin are perpendicular to the scattering plane  $V(z) = 2\pi\hbar^2 nb/m_n \mp \mu_n M(z)$ , where  $\mp$  is for spin up and down, respectively,  $m_n$  is the neutron mass,  $n$  is the number density of nuclei,  $b$  is the average scattering length of the nucleus,  $\mu_n$  is the neutron magnetic moment, and  $M(z)$  is the spatially varying sample magnetization. Thus, the diamagnetism within the superconductor generates a different potential for spin-up and spin-down neutrons.

Previous spin-polarized neutron reflectivity experiments<sup>12-14</sup> that measured  $\lambda_L$  were performed at low magnetic field in order to avoid the introduction of vortices, which reduces the magnetization of the sample. However, as shown by the calculations in Fig. 1, the presence of vortices within the superconductor does not necessarily eliminate the difference in potential for spin-up and spin-down neutrons. Of course, the detailed shape of the potential will depend on the specific vortex distribution. This suggests that spin-polarized neutron reflection techniques should be able to observe the presence of vortices as well as obtain information on their spatial distribution in the direction perpendicular to the surface.

## II. EXPERIMENTAL RESULTS

The experiment was performed on a 6000 Å thick  $\text{YBa}_2\text{Cu}_3\text{O}_{7-x}$  film, grown by magnetron sputtering,<sup>15</sup> with the  $c$  axis perpendicular to the (1 cm × 1 cm)  $\text{SrTiO}_3$  substrate surface. The resistivity, measured on similar samples by the four-probe technique, was 208  $\mu\Omega$  cm at room temperature with an onset to superconductivity at 89.8 K and a transition width of 0.8 K. The neutron experiment utilized a closed-cycle refrigerator to cool the sample to 10 K in zero magnetic field. Subsequently, a magnetic field was applied parallel to the surface, as shown in the inset to Fig. 1, using an electromagnet. The experiments were performed using the GANS reflectometer<sup>16</sup> at the Missouri University Research Reactor and the specular reflectivity was measured separately for spin-up and spin-down incident neutrons (a polarization analyzer was not used) having a wavelength of  $\lambda = 2.35$  Å. The angular divergence of the incoming beam was 0.02° and the beam width at sample position was 0.23 mm. The rms surface roughness of the specimen  $170 \pm 30$  Å was determined by neutron reflectivity and atomic force microscopy measurements.

Figure 2 (a) shows the measured spin-up and spin-down reflectivities near the critical angle for total external reflection at an applied field of 2400 Oe. The magnetic effects are observed more easily by plotting  $\Delta R/\bar{R}$ , which is the difference of the spin-up and spin-down reflectivities divided by their average, as shown in Fig. 2(b). From these data alone it would be difficult, without a model calculation, to determine the relative contributions from the London penetration at the surface and the vortices. However, the two contributions are clearly distinguished by measuring the field dependence.

Figure 3 shows the extremal value of  $\Delta R/\bar{R}$  measured as

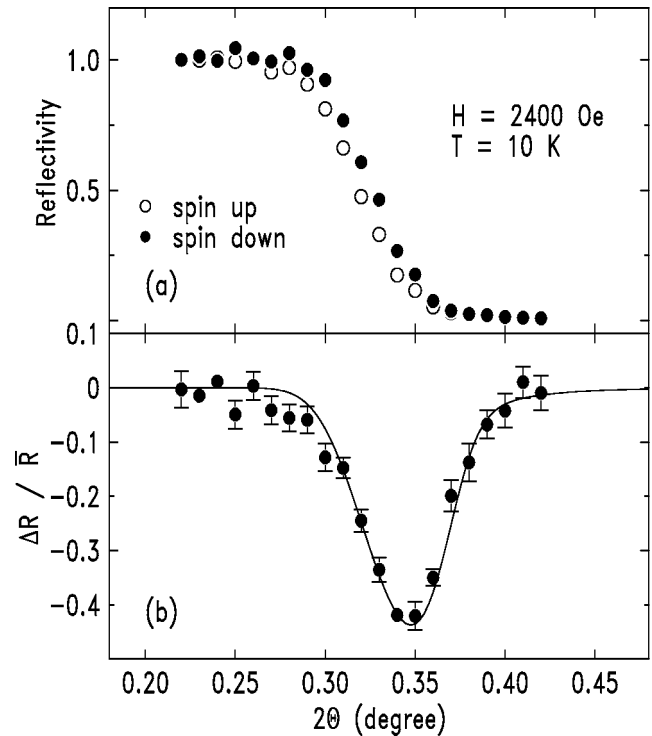


FIG. 2. (a) shows the spin-up and spin-down neutron reflectivities for  $H=2400$  Oe at 10 K. (b)  $\Delta R/\bar{R}$ , which is the reflectivity difference of the spin-up and spin-down reflectivity divided by their average, is obtained from the data in (a). The solid curve is a best fit to the model described in the text (convoluted with the instrumental resolution and corrected for the polarization efficiency).

a function of applied field. Initially, at low field, there is a nearly linear change in  $\Delta R/\bar{R}$  due to the London penetration; however, at higher field, the slope of  $\Delta R/\bar{R}$  changes as vortices are generated. The hysteresis shape unambiguously demonstrates that vortices can be detected by spin-polarized neutron reflection. Even when the applied field is reduced to

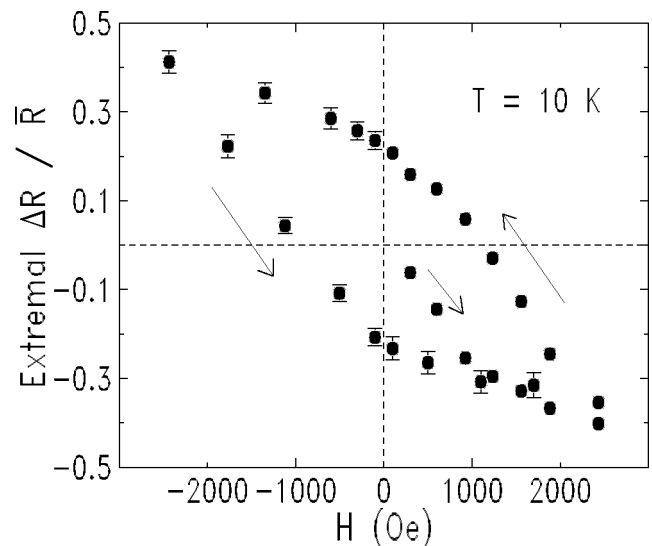


FIG. 3. The extremal  $\Delta R/\bar{R}$  measured as a function of applied field for a zero-field-cooled sample. The arrows indicate the order in which the data were taken.

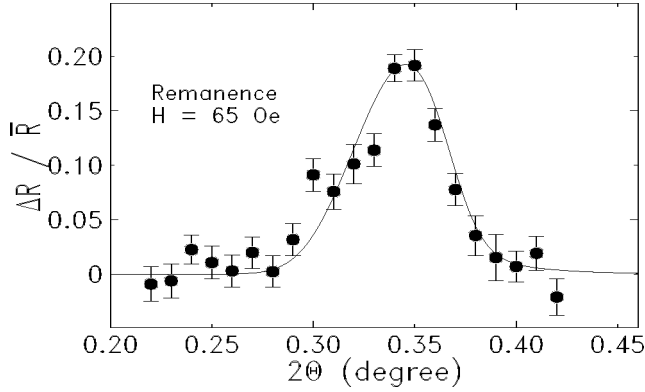


FIG. 4.  $\Delta R/\bar{R}$  was measured at 65 Oe and 10 K after a field of 2400 Oe had been applied. The large  $\Delta R/\bar{R}$  having opposite sign to the data in Fig. 2(b) indicates a remanent condition with trapped vortices.

a small value (65 Oe) there is a large spin-polarized signal (see Fig. 4), which is opposite in sign to that of Fig. 2(b), due to the remanent condition where vortices are trapped in the sample.

### III. THEORETICAL MODEL

In order to analyze the experimental results we developed a model of the reflectivity for a given spatial distribution of vortices. The field penetration at both surfaces of the film as well as the vortices within the film contribute to the spin-polarized reflectivity. First we obtain the spatial variation of the magnetic field in the sample by solving the London equation<sup>17</sup> with  $N$  vortices

$$\vec{B}(\vec{r}) + \lambda_L^2 \nabla \times \nabla \times \vec{B}(\vec{r}) = \vec{\Phi}_0 \sum_{p=1}^{p=N} \delta^{(2)}(\vec{r} - \vec{r}_p), \quad (3.1)$$

where  $\vec{\Phi}_0$  is the flux of a single vortex having a magnitude  $\Phi_0 = ch/2e = 20.679$  Oe  $\mu\text{m}^2$ ,  $\vec{r}_p$  is the position of  $p$ th vortex, and  $\delta^{(2)}(\vec{r})$  is a two-dimensional (2D) delta function. A magnetic field applied parallel to the film surface leads to

$$B_x(\vec{r}) = B_h(\vec{r}) + \frac{\Phi_0}{2\pi\lambda_L^2} \int d^{(2)}\vec{r}' n_v(\vec{r}') K_0\left(\frac{|\vec{r} - \vec{r}'|}{\lambda_L}\right), \quad (3.2)$$

where  $n_v(\vec{r}) = \sum_{p=1}^{p=N} \delta^{(2)}(\vec{r} - \vec{r}_p)$  is the vortex density and  $K_0(r)$  is a modified Bessel function.  $B_h(\vec{r})$  is the homogeneous solution to Eq. (3.1) that is used to satisfy the boundary condition  $\vec{B} = \mu_0 H \hat{x}$  at both interfaces.

Due to the condition of specular reflection, only the field averaged over the  $\hat{y}$  direction is used. Integrating Eq. (3.2) over  $y$  and applying the boundary condition gives

$$\begin{aligned} \bar{B}_x(z) = & \mu_0 H \frac{\cosh(z/\lambda_L)}{\cosh(t/2\lambda_L)} + \frac{\Phi_0}{2\lambda_L} \int_{-t/2}^{t/2} dz' \bar{n}_v(z') \\ & \times \left\{ e^{-|z-z'|/\lambda_L} - e^{(2z-t)/2\lambda_L} \frac{\sinh[(2z'+t)/2\lambda_L]}{\sinh(t/\lambda_L)} \right. \\ & \left. + e^{-(2z+t)/2\lambda_L} \frac{\sinh[(2z'-t)/2\lambda_L]}{\sinh(t/\lambda_L)} \right\}, \quad (3.3) \end{aligned}$$

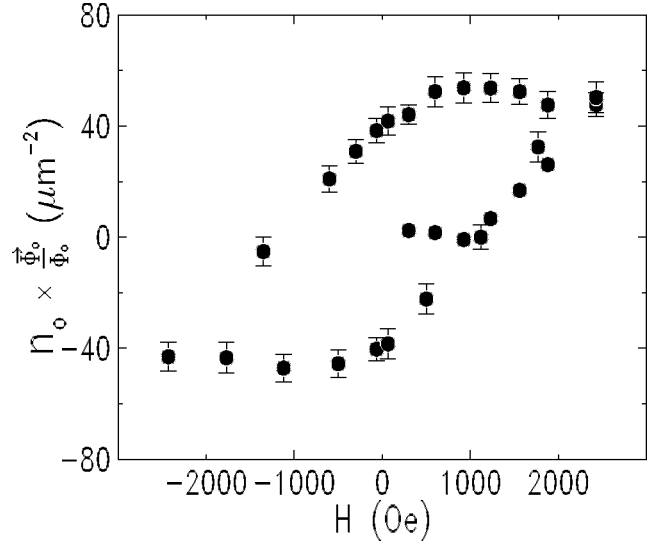


FIG. 5. The average density of vortices are extracted from the data in Fig. 3, using the model discussed in the text.

where  $t$  is the film thickness.  $\bar{n}_v(z) = (1/L) \int_{-L/2}^{L/2} dy n_v(\vec{r})$  is the 1D spatially varying vortex density, where  $L$  is the lateral dimension of the sample. The first term in Eq. (3.3) is just London penetration from the interfaces. The first term in the integrand is the free-space contribution of the vortices and the last two terms in the integrand arise from the image field of the vortices.

With  $M(z) = \bar{B}_x(z)/\mu_0 - H$  determined from Eq. (3.3), the scattering potential  $V(z)$  can be calculated and the 1D Schrödinger equation is solved numerically to obtain the spin-dependent reflectivity. Thus, it is seen that the spin-polarized reflectivity depends explicitly on the 1D vortex density  $\bar{n}_v(z)$ . To compare with the experimental data, the result is convoluted with the instrumental (Gaussian) resolution as well as corrected for beam foot print and polarization efficiency.

### IV. ANALYSIS AND DISCUSSION

In the analysis, the London penetration length was taken to be 1400 Å,<sup>14</sup> although, it was found that the results in Fig. 5 were relatively insensitive to the precise value of  $\lambda_L$ . It was also assumed that the vortices are distributed uniformly through the sample and this is justified for two reasons. First, our calculations show that for intermediate field values on the hysteresis loop, large changes in the shape of  $\Delta R/\bar{R}$  vs  $2\theta$  will occur if vortices are localized near the center of the film; this was not observed in our experiments, suggesting that the vortices are distributed uniformly at intermediate field values. Secondly, at other field values the data have limited sensitivity to the shape of the vortex distribution because these experiments were obtained at low  $q_z$  (dictated by the large surface roughness<sup>18</sup>) where the average scattering density is effectively measured in this limit (see below). The solid curves in Fig. 2(b) and Fig. 4 are a best fit to the model. The width of these curves are essentially resolution limited and the shape does not change with applied field.

Using the data in Fig. 3, the field dependence of the average vortex density  $n_0$  was obtained from this analysis and

the results are shown in Fig. 5. Initially there are no vortices in the zero-field-cooled sample and vortices first enter the sample near  $1050 \pm 100$  Oe. Upon increasing the field above this value there is a linear increase in the vortex density. As the field is reduced there is little change in the vortex density until rather low field, indicative of a barrier for vortices to exit the sample. The slope of the linear portions is the same for increasing or decreasing fields and is determined to be  $\Delta n_0/\Delta H = 0.036 \pm 0.006 \text{ Oe}^{-1} \mu\text{m}^{-2}$ . Assuming a uniform distribution of vortices, applying the appropriate boundary condition and assuming the average magnetization does not change with applied field ( $\Delta \bar{M}/\Delta H = 0$ ), we would expect  $\Delta n_0/\Delta H \approx 1/\Phi_0 = 0.05 \text{ Oe}^{-1} \mu\text{m}^{-2}$  for our sample configuration (thickness  $\approx 4\lambda_L$ ). The experimental value is slightly smaller, consistent with  $\Delta \bar{M}/\Delta H \sim -0.14$ .

We now use our model to demonstrate that spin-polarized neutron reflectivity can, in principle, reveal the spatial distribution of vortices in the direction perpendicular to the surface. Figure 6 shows  $\Delta R/\bar{R}$  calculated for three different distributions of vortices having the same average vortex density: vortices localized on a plane through the center of the film, vortices localized on two planes, and vortices spread over a Gaussian distribution. Near the critical angle ( $2\theta_c \sim 0.32^\circ$ ) the curves exhibit little change with the vortex distribution and, thus, explains why the present experiment provides only the average vortex density. However, a clear difference between the curves in Fig. 6 emerges at higher angle. This sensitivity to the spatial distribution of vortices is intrinsic to neutron reflectivity since, in the limit of the Born approximation, the reflectivity is related to the Fourier transform of the scattering density. As a practical matter, it may be difficult to obtain high  $q_z$  data in materials which have a large surface roughness, such as some oxide superconductors;<sup>18</sup> increasing the film thickness also exacerbates the problem since roughness often increases with thickness. However, there are many thin-film materials, particularly conventional superconductors, that can be grown with sufficiently smooth surfaces. Indeed, a recent spin-polarized neutron reflectivity study of  $\lambda_L$  in Nb was performed at higher  $q_z$ .<sup>13</sup>

In conclusion, we have shown that spin-polarized neutron reflectivity can probe vortices in a geometry which is generally inaccessible by other techniques. In particular, it has the capability to study vortices that are parallel to the surface and

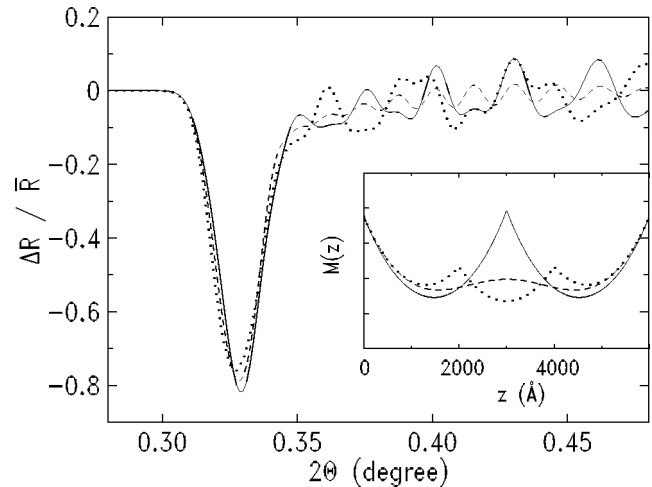


FIG. 6. Calculation of  $\Delta R/\bar{R}$  for three different distributions of vortices (same average density). The inset shows the spatially varying magnetization for each case. (Solid curve) vortices localized on the plane through the center of the sample, (dotted curve) vortices localized on two planes ( $\pm 1000 \text{ \AA}$  about the center), and (dashed curve) vortices spread over a Gaussian distribution with standard deviation  $1000 \text{ \AA}$ . The parameters used for the solid line in Fig. 2(b) were also used for this calculation except with four times better resolution.

it is sensitive to the one-dimensional spatially varying vortex density. Long-range order of the vortices is not required. This technique is uniquely suited to investigate the interaction of vortices with the surface. For example, recent magnetization experiments<sup>19</sup> have suggested that vortices order in thin films due to vortex-surface interactions. Such vortex-surface ordering should be observable by neutron reflection.

#### ACKNOWLEDGMENTS

Support (P.F.M., S.W.H.) from the Midwest Superconductivity Consortium (MISCON) under the U.S. DOE Grant No. DE-FG02-90ER45427, the NSF DMR Grant No. 96-23827, and (L.H.G., E.P.) from the NSF DMR Grant No. 94-21957, and ONR Grant No. N-00014-95-1-0831 is gratefully acknowledged. We thank E. Fullerton for useful discussions and D.H. Lowndes for help in understanding the surface roughness of oxide superconductors.

\*Present address: Spallation Neutron Source, Oak Ridge National Laboratory, Oak Ridge, TN 37831.

†Author to whom correspondence should be addressed.

<sup>1</sup>G. Blatter, M. V. Feigel'man, V. B. Geshkenbein, A. I. Larkin, and V. M. Vinokur, *Rev. Mod. Phys.* **66**, 1125 (1994).

<sup>2</sup>G. W. Crabtree and D. R. Nelson, *Phys. Today* **50** (4), 39 (1997).

<sup>3</sup>Matthew F. Schmidt, N. E. Israeloff, and A. M. Goldman, *Phys. Rev. Lett.* **70**, 2162 (1993).

<sup>4</sup>J. W. Lynn, N. Rosov, T. E. Grigereit, H. Zhang, and T. W. Clinton, *Phys. Rev. Lett.* **72**, 3413 (1994).

<sup>5</sup>P. L. Gammel, D. J. Bishop, G. J. Dolan, J. R. Kwo, C. A. Murray, L. F. Schneemeyer, and J. V. Waszczak, *Phys. Rev. Lett.* **59**, 2592 (1987).

<sup>6</sup>K. Harada, T. Matsuda, J. Bonevich, M. Igarashi, S. Kondo, G.

Pozzi, U. Kawabe, and A. Tonomura, *Nature (London) (London)* **360**, 51 (1992).

<sup>7</sup>H. F. Hess, R. B. Robinson, R. C. Dynes, J. M. Valles, Jr., and J. V. Waszczak, *Phys. Rev. Lett.* **62**, 214 (1989).

<sup>8</sup>A. M. Chang, H. D. Hallen, L. Harriott, H. F. Hess, H. L. Kao, J. Kwo, R. E. Miller, R. Wolfe, and J. van der Ziel, *Appl. Phys. Lett.* **61**, 1974 (1992).

<sup>9</sup>A. Tonomura, *Adv. Phys.* **41**, 59 (1992); J. E. Bonevich, K. Harada, T. Matsuda, H. Kasai, T. Yoshida, G. Pozzi, and A. Tonomura, *Phys. Rev. Lett.* **70**, 2952 (1993).

<sup>10</sup>D. K. Christen, H. R. Kerchner, S. T. Sekula, and P. Thorel, *Phys. Rev. B* **21**, 102 (1980); D. Cribier, B. Jacrot, L. M. Rao, and B. Farnoux, *Phys. Lett.* **9**, 106 (1964); E. M. Forgan, D. Mck. Paul, H. A. Mook, P. A. Timmins, H. Keller, S. Sutton, and J. S.

- Abell, *Nature (London)* **343**, 735 (1990); U. Yaron, P. L. Gammel, G. S. Boebinger, G. Aeppli, P. Schiffer, E. Bucher, D. J. Bishop, C. Broholm, and K. Mortensen, *Phys. Rev. Lett.* **78**, 3185 (1997).
- <sup>11</sup>C. F. Majkrzak, *Physica B* **221**, 342 (1996).
- <sup>12</sup>G. P. Felcher, R. T. Kampwirth, K. E. Gray, and R. Felici, *Phys. Rev. Lett.* **52**, 1539 (1984); D. A. Korneev, L. P. Chernenko, A. V. Petrenko, N. I. Balalykin, and A. V. Skrypnik, *Pis'ma Zh. Eksp. Teor. Fiz.* **55**, 653 (1992) [*JETP Lett.* **55**, 683 (1992)].
- <sup>13</sup>H. Zhang, J. W. Lynn, C. F. Majkrzak, S. K. Satija, J. H. Kang, X. D. Wu, *Phys. Rev. B* **52**, 10 395 (1995).
- <sup>14</sup>A. Mansour, R. O. Hilleke, G. P. Felcher, R. B. Lainbowitz, P. Chaudhari, and S. S. P. Parkin, *Physica B* **156&157**, 867 (1989); R. Felici, J. Penfold, R. C. Ward, E. Olsi, and C. Maticotta, *Nature (London)* **329**, 523 (1987); S. V. Gaponov, E. B. Dokukin, D. A. Korneev, E. B. Klyuenkov, W. Löbner, V. V. Pasyuk, A. V. Petrenko, Kh. Rzhany, and L. P. Chernenko, *Pis'ma Zh. Eksp. Teor. Fiz.* **49**, 277 (1989) [*JETP Lett.* **49**, 316 (1989)]; V. Lauter-Pasyuk, H. J. Aksenov, E. L. Kornilov, A. V. Petrenko, and P. Leiderer, *Physica B* **248**, 166 (1998).
- <sup>15</sup>L. H. Greene, B. G. Bagley, W. L. Feldman, J. B. Barner, F. Shokoochi, P. F. Miceli, B. J. Wilkins, V. Pendrick, D. Kalokitis, and A. Fathy, *Appl. Phys. Lett.* **59**, 1629 (1991); J. Lesueur, L. H. Greene, W. L. Feldman, and A. Inam, *Physica C* **191**, 325 (1992).
- <sup>16</sup>H. Kaiser, K. Hamacher, R. Kulasekera, W.-T. Lee, J. F. Ankner, B. DeFacio, P. Miceli, and D. L. Worcester, in *Inverse Optics III*, SPIE Conf. Proc. Vol. **2241** (SPIE, Bellingham, WA, 1994), pp. 78–89.
- <sup>17</sup>P. G. de Gennes, *Superconductivity of Metals and Alloys* (Addison-Wesley, New York, 1989).
- <sup>18</sup>S.-W. Han, J. A. Pitney, P. F. Miceli, M. Covington, L. H. Greene, M. J. Godbole, and D. H. Lowndes, *Physica B* **221**, 235 (1996).
- <sup>19</sup>S. H. Brongersma, E. Verweij, N. J. Koeman, D. G. de Groot, R. Griessen, and B. I. Ivlev, *Phys. Rev. Lett.* **71**, 2319 (1993); I. K. Schuller, J. Guimpel, and Y. Bruynseraede, *MRS Bull.* **15** (2), 29 (1990).